Viscoelastic Stress/Strain Behavior of Pharmaceutical Tablets: Analysis during Unloading and Postcompression Periods

EDWARD G. RIPPIE ˣ **and DOUGLAS W. DANIELSON** *

Received May 15, 1980, from the *Department of Pharmaceutics, College of Pharmacy, University of Minnesota, Minneapolis, MN 55455.* Accepted for publication November 11, 1980. *Present address: Merrell National Laboratories, Cincinnati, OH 45215.

Abstract □ The processes of nonequilibrium generation and decay of axial and radial stresses within tablet compacts were analyzed in terms of three-dimensional linear viscoelastic theory. A rotary tablet press was instrumented to measure punch and die wall stresses during the compression and postcompression periods. Following compression, tablets were permitted to remain at the compression site within the die, and the die wall stress was followed. Microcrystalline cellulose, spray-processed lactose, and sulfacetamide are known to have different compression characteristics and were found to differ significantly in their viscoelastic parameters. Compacts assumed their final viscoelastic state prior to the time of punch separation. Theory permits separation of material behavior into dilation and distortion components. Dilation, thought to be dependent on voids, was elastic in all cases. Distortion effects could be described well by a Kelvin solid model. Results indicate that viscoelastic properties are functions of compression conditions and may be useful in adjusting compression conditions to avoid problems such as capping.

Keyphrases □ Viscoelastic behavior—analysis of tablets during unloading and postcompression □ Tablet formulation—analysis of viscoelastic behavior during unloading and postcompression □ Compression cycle—analysis of viscoelastic behavior during tablet formulation

The compression of powdered or granular material into a cohesive mass during the formation of a pharmaceutical tablet is a complex and irreversible dynamic process, in contrast to its apparent simplicity. Mechanically, the process consists of imposing a strain on the powder by progressively confining it to a diminishing volume, reaching approximately that of the completed tablet. The dimensional constraints imposed by the punches and die then are removed, and the compact is allowed to relax. The compacted material exerts stress against the punches and die during this process in response to the imposed strain. For this reason, useful information concerning the fundamental structure of tablets is available from compression stress/strain data, as reflected by the substantial volume of literature in the area.

In the present investigation, three-dimensional viscoelastic models of both the unloading portion of the compression event and the postcompression relaxation period were studied. They were examined for their utility in the analysis of internal structural behavior and changes that result from tablet compression. For this purpose, axial and radial stress/strain data were obtained under nonequilibrium conditions at normal operating speeds in a rotary tablet machine and were interpreted *via* these models.

BACKGROUND

The stress/strain behavior observed in tablet compaction is a composite of effects arising from primary particle reorientation, elastic deformation, particle fracture, viscous and/or plastic flow, and the formation and breaking of interparticulate bonds. Some of these processes are time dependent and occur at various rates over the period of tablet formation. Therefore, the compact is not at stress/strain equilibrium during the compression event. Thus, the physical characteristics of the finished tablet may be expected to depend on the strain rate profile imposed by the tablet machine, the viscoelastic properties of the compact, and the resultant stresses during compaction and ejection from the die.

Arguments and evidence (1, 2) have indicated that the nature of stress release during decompression and stress unloading may be a major factor responsible for the success or failure of tablet formation. Studies of the quasistatic (2–5) and dynamic (6–8) loading characteristics of pharmaceutical compacts support the widely held view that substantial internal mass flow occurs during tableting. This flow is manifested as stress relaxation under constant (1) and changing (8–11) external strain. The strains applied during compression require the compacted material to yield or flow and to produce stresses that can result from four fundamental processes: elastic yield, viscous flow, plastic deformation, and mass acceleration. The meanings of these terms may differ somewhat in various contexts and will be defined as follows for this discussion.

Elastic yield is the instantaneous and totally reversible response to an applied load. It may be represented in linear form by a massless spring having no inertia. Viscous flow is defined, in its linear form, as Newtonian flow and is symbolized by a dashpot for which the rate of strain is directly proportional to the applied stress. Irreversible strains that result from stresses above a threshold value (elastic limit) are termed plastic deformations. The stress necessary to maintain motion, once begun in a perfectly plastic material, is independent of the strain rate. This idealized plastic behavior is analogous to a weight being slid across a level surface after static friction has been overcome. Inertial forces resulting from the movement of mass within a tablet also contribute to its stress/strain behavior during compression. However, because of the small masses and low accelerations involved, these forces are negligible and may be disregarded.

A model based on brittle fracture as the mechanism for tablet consolidation (12) has been applied to granular material subject to quasistatic stress loading and unloading. However, it is generally recognized that some plastic flow occurs at points of interparticulate contact during compression. Due to the force-concentrating effect of asperities (5), overall pressures required for this process are much lower than would produce plastic flow of the bulk material. This phenomenon generally has been termed "microsquashing" in the powder technology literature and is commonly thought to occur when particles are smaller than 1 mm. If only brittle fracture occurred during compaction, the result would be a finer powder rather than a coherent compact. However, strong compacts can be made of brittle materials even though extensive fragmentation of the primary particles is observed (13). A more general model (14), based on plastic yielding, is compatible with the consolidation pattern observed in isostatic loading. Both of these models are intended to apply only to quasistatic loading. It was demonstrated (8) that the punch to die wall pressure behavior observed during dynamic compaction in a rotary tablet press is markedly different than that observed during quasistatic loading.

In practice, loading and unloading of stresses within the tablet and its powdered precursor are accomplished in a few milliseconds. It was suggested that the resultant transient processes occur in stages during this brief period (15). A decrease in voids is most probably caused by interparticulate slippage in Stage I. Stage II is characterized by the formation

0022-3549/81/0500-0476$01.00/0

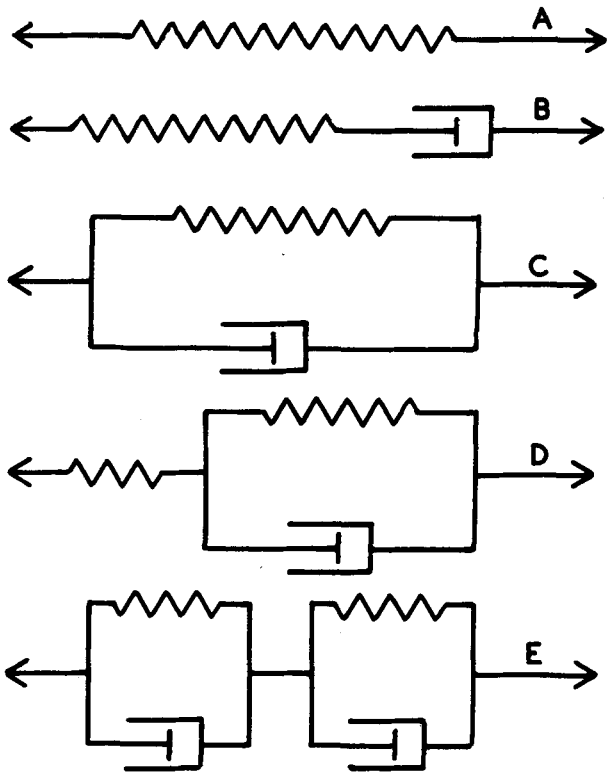

Figure 1—*Fundamental viscoelastic models. Key: A, elastic solid; B, Maxwell fluid; C, Kelvin solid; D, three-parameter solid; and E, four-parameter solid.*

of temporary struts, columns, and vaults protecting small voids and generally supporting the imposed load. In Stage III, this structure fails by particle fracture or plastic flow. The final condition is reached in Stage IV when the structure formed is strong enough to support the imposed load and any further reduction in volume of the compact involves the normal compressibility of the solid material. At this stage, any permanent decrease in the voids of a still porous compact can only be achieved by exceeding the crushing strength of the structure and/or by plastic deformation.

Depending on the kinetics of the various fundamental processes involved, Stage IV may not be reached until the punches are receding and stress unloading is well underway. It may be postulated that the structure responsible for the viscoelastic properties of the tablet are established during this final stage. These properties would then be the cumulative result of changes brought about during compact formation. Thus, they may be expected to be a function of the stress/strain history of the tablet and could change if the conditions of earlier stages were recreated as, for example, by recompression.

In the present studies, measurements of the viscoelastic behavior of the compact during the latter portion of the unloading phase of compaction are combined with results obtained immediately after punch separation but before ejection from the die. The viscoelastic parameters, derived from data obtained under these two sets of conditions, are useful in predicting evolutionary changes in the tablet prior to ejection. This prediction is important if the stress/strain condition of the tablet upon ejection from the die is to be calculated from information gathered earlier in the cycle.

THEORETICAL

Viscoelastic Constitutive Equations in One Dimension—The time-dependent behavior of viscoelastic materials can be closely modeled by the use of combinations of discrete elastic and viscous elements (16, 17). The arrangement of the spring and dashpot elements within the models determines their characteristics and whether the material is a viscoelastic fluid or solid. For example, the coupling of a spring and dashpot in series is termed a Maxwell fluid. When the two elements are coupled in parallel, the model is a Kelvin solid. If a second spring is added in series to the Kelvin solid, the result is a standard three-parameter solid. These and other models used in this investigation are illustrated in Fig. 1. The equation of a linear elastic element, conforming to Hooke's law, is:

$$\sigma = F\epsilon \qquad \text{(Eq. 1)}$$

where σ and ϵ are the stress and strain, respectively, and F is the modulus for the spring. The viscous behavior of a Newtonian dashpot is given by:

$$\sigma = G\dot{\epsilon} \qquad \text{(Eq. 2)}$$

where $\dot{\epsilon}$ is $d\epsilon/dt$, the strain rate, and G is the viscous coefficient. A tablet, left in the die after compression, exerts a residual die wall stress indefinitely, and a solid viscoelastic model, such as a Kelvin or a three-parameter solid, is needed to describe this behavior.

The constitutive equation of a Kelvin solid, where a spring and dashpot are coupled in parallel, is based on an equal strain of the two elements. Thus, the stress is distributed between them so that, from Eqs. 1 and 2:

$$\sigma = F\epsilon + G\dot{\epsilon} \qquad \text{(Eq. 3)}$$

More complicated models can be built systematically in the pattern shown in Fig. 1. The differential equations of these and other types of viscoelastic models (17) have the general form:

$$\sigma + p_1\dot{\sigma} + p_2\ddot{\sigma} + \cdots = q_0\epsilon + q_1\dot{\epsilon} + q_2\ddot{\epsilon} + \cdots \qquad \text{(Eq. 4)}$$

where $p_0 \equiv 1$. In the case of the Kelvin solid, $p_{i\neq 0} = 0$, $q_0 = F$, $q_1 = G$, and $q_{i\geq 2} = 0$. For other more complicated models, the coefficients p_i and q_i are various functions of the elastic and viscous constants corresponding to the constituent springs and dashpots. It is convenient to write these equations in differential operator notation:

$$P\sigma = Q\epsilon \qquad \text{(Eq. 5)}$$

where P and Q are defined as:

$$P = \sum p_i\, d^i/dt^i \qquad \text{(Eq. 6)}$$

$$Q = \sum q_i\, d^i/dt^i \qquad \text{(Eq. 7)}$$

and where, for a Kelvin solid:

$$P = 1 \qquad \text{(Eq. 8)}$$

$$Q = q_0 + q_1\, d/dt \qquad \text{(Eq. 9)}$$

Three-Dimensional Viscoelastic Behavior—The theory described thus far is adequate only when stresses and strains are in just one dimension. For the case of a tablet under compaction in a rigid die, axial

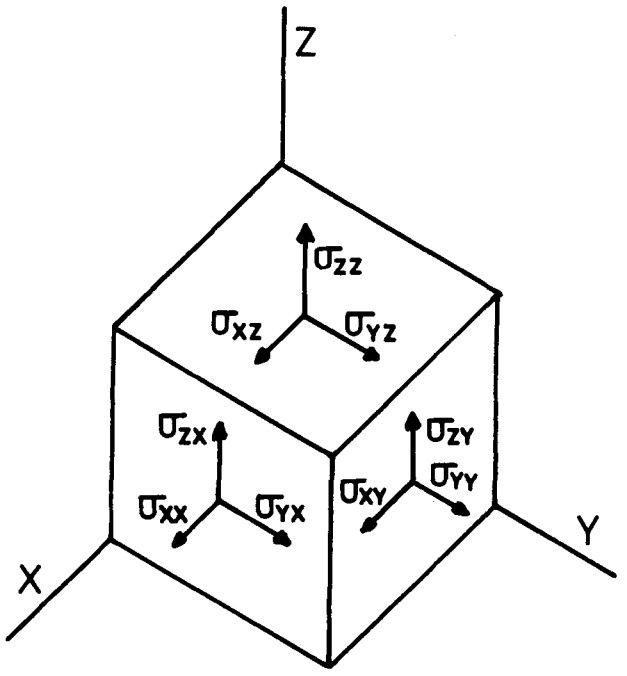

Figure 2—*Stress components acting on a cubical element within a stressed body.*

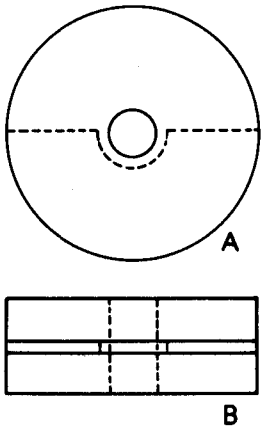

Figure 3—*Schematic drawing of tablet die, showing top (A) and side (B) views.*

strains are imposed by the punches and radial strains result, in part, from the lateral wedging of the particles as they are driven together. A more general expression of viscoelastic behavior than that given by Eqs. 5–7 is needed to account for processes occurring in three dimensions.

Three-dimensional viscoelastic theory can be developed from a consideration of the stresses and strains experienced by an infinitesimal cubical element within a stressed and strained solid body. Nine stress components, as illustrated in Fig. 2, comprise the stress tensor, $\hat{\sigma}$:

$$\hat{\sigma} = \begin{bmatrix} \sigma_{xx} & \sigma_{xy} & \sigma_{xz} \\ \sigma_{yx} & \sigma_{yy} & \sigma_{yz} \\ \sigma_{zx} & \sigma_{zy} & \sigma_{zz} \end{bmatrix} \quad \text{(Eq. 10)}$$

where σ_{ij} denotes the stress in the ith direction on the jth face of the cube. Thus, where $i = j$, the stresses are normal to the surface; where $i \neq j$, shear stresses are indicated. If the cube is in moment equilibrium and not undergoing angular acceleration, $\sigma_{ij} = \sigma_{ji}$, so that there are six independent stress components under these conditions.

The stress tensor can be split into two parts, as in Eq. 11, so that the stresses leading to isostatic compression or dilation, $\hat{s}$, can be separated from those, $\hat{S}$, producing distortion of shape:

$$\hat{\sigma} = \hat{s} + \hat{S} \quad \text{(Eq. 11)}$$

where:

$$\hat{s} = \begin{bmatrix} s & 0 & 0 \\ 0 & s & 0 \\ 0 & 0 & s \end{bmatrix} \quad \text{(Eq. 12)}$$

and:

$$\hat{S} = \begin{bmatrix} S_{xx} & S_{xy} & S_{xz} \\ S_{yx} & S_{yy} & S_{yz} \\ S_{zx} & S_{zy} & S_{zz} \end{bmatrix} \quad \text{(Eq. 13)}$$

The isostatic stress components, s, are each taken as equal to $(\sigma_{xx} + \sigma_{yy} + \sigma_{zz})/3$. It follows from Eqs. 10–13 that $S_{xx} + S_{yy} + S_{zz} = 0$.

A similar operation may be performed on the strain tensor, $\hat{\epsilon}$, resolving it into isostatic, $\hat{e}$, and distortional, $\hat{E}$, strain tensors:

$$\begin{bmatrix} \epsilon_{xx} & \epsilon_{xy} & \epsilon_{xz} \\ \epsilon_{yx} & \epsilon_{yy} & \epsilon_{yz} \\ \epsilon_{zx} & \epsilon_{zy} & \epsilon_{zz} \end{bmatrix} = \begin{bmatrix} e & 0 & 0 \\ 0 & e & 0 \\ 0 & 0 & e \end{bmatrix} + \begin{bmatrix} E_{xx} & E_{xy} & E_{xz} \\ E_{yx} & E_{yy} & E_{yz} \\ E_{zx} & E_{zy} & E_{zz} \end{bmatrix} \quad \text{(Eq. 14)}$$

where $e = (\epsilon_{xx} + \epsilon_{yy} + \epsilon_{zz})/3$ and $E_{xx} + E_{yy} + E_{zz} = 0$.

For an isotropic viscoelastic material, $\hat{s}$ causes only volumetric changes, while only distortional changes are produced by $\hat{S}$. This behavior can be expressed by constitutive equations, analogous to Eq. 5, in which the volumetric and distortional effects are separated:

$$P''\hat{s} = Q''\hat{e} \quad \text{(Eq. 15)}$$

where:

$$P'' = \sum p_i'' \, d^i/dt^i \quad \text{(Eq. 16)}$$

$$Q'' = \sum q_i'' \, d^i/dt^i \quad \text{(Eq. 17)}$$

and:

$$P'\hat{S} = Q'\hat{E} \quad \text{(Eq. 18)}$$

where:

$$P' = \sum p_i' \, d^i/dt^i \quad \text{(Eq. 19)}$$

$$Q' = \sum q_i' \, d^i/dt^i \quad \text{(Eq. 20)}$$

The operator pairs P'' and Q'' and P' and Q' are totally independent of each other under these conditions. The nature of the viscoelastic material, *i.e.*, elastic solid, Kelvin solid, *etc.*, is expressed in Eqs. 15 and 18 *via* the operator pairs. For these reasons, it is possible to construct models in which the isostatic behavior is different from that proposed for distortion.

Uniaxial Stress and Strain—In applying three-dimensional theory to viscoelastic behavior, it is useful to consider the special case of a simple tension, σ_{xx}, applied to a three-dimensional body. The diagonal elements of $\hat{s}$ each become equal to $\sigma_{xx}/3$, and the nonzero elements of $\hat{S}$ are then $S_{xx} = 2\sigma_{xx}/3$ and $S_{yy} = S_{zz} = -\sigma_{xx}/3$. The strains resulting from these stresses appear as an elongation, ϵ_{xx}, coupled with transverse contractions, $\epsilon_{yy} = \epsilon_{zz}$, which contribute to $\hat{e}$ and $\hat{E}$ so that $e = (\epsilon_{xx} + 2\epsilon_{yy})/3$, $E_{xx} = 2(\epsilon_{xx} - \epsilon_{yy})/3$, and $E_{yy} = E_{zz} = -(\epsilon_{xx} - \epsilon_{yy})/3$. Furthermore, if it is assumed that the operators P and Q are linear and time invarient, Eqs. 15 and 18 may be written in terms of the applied uniaxial stress:

$$(P''Q' + 2P'Q'')\sigma_{xx} = 3Q'Q''\epsilon_{xx} \quad \text{(Eq. 21)}$$

$$(P''Q' - P'Q'')\sigma_{xx} = 3Q'Q''\epsilon_{yy} = 3Q'Q''\epsilon_{zz} \quad \text{(Eq. 22)}$$

By analogous arguments applied to Eqs. 15 and 18, and with the same restrictions on P and Q, the following equations may be derived for the case of an applied uniaxial strain, ϵ_{xx}:

$$(P'Q'' + 2P''Q')\epsilon_{xx} = 3P'P''\sigma_{xx} \quad \text{(Eq. 23)}$$

$$(P'Q'' - P''Q')\epsilon_{xx} = 3P'P''\sigma_{yy} = 3P'P''\sigma_{zz} \quad \text{(Eq. 24)}$$

More detailed expositions (16, 17) of fundamental linear viscoelastic theory are available; however, the theory outlined here suffices for the present study. With the limitations and assumptions implicit in their derivation, Eqs. 21–24 can be applied, in linear combination, in modeling the process of tablet formation.

EXPERIMENTAL

Press Instrumentation—Tablets were compressed using flat-faced punches on a rotary tablet machine[1]. A single station was instrumented with resistance strain gauges to monitor both die wall and punch stresses. All other stations were blank. The ejection cam was removed so that the tablet remained in the die after compaction, and its stress relaxation could be observed over an indefinitely extended period. Punch stress was measured by four strain gauges[2] attached to the lower compression roller support rod in a Poisson configuration. The gauges were activated in a direct-current Wheatstone bridge coupled[3] to the strain-gauge amplifier[4].

The die recess in the active station was enlarged to accommodate a specially made 9.525-mm laminar tablet die (Fig. 3). Mating surfaces of the three die layers were surface ground to ensure a close fit. The center layer, 1.5 mm thick, had a reduced wall thickness of 3.2 mm for half of its circumference. The upper and lower surfaces of this thin-walled segment each were ground down 5 μm to provide clearance for free radial expansion of the arch under stress. Extrusion of tablet material into this space was negligible, and only infrequent disassembly was needed for cleaning. An active strain gauge[5] was bonded to the arch and a second gauge was bonded to the lower die segment for temperature compensation. The Wheatstone bridge was completed internally, using precision wound resistors[6], within the strain-gauge amplifier to which it was hard wired[3].

Amplifier output signals were displayed on a storage oscilloscope[7], and stress measurements were made[8] from photos[9] of the traces. A typical

[1] Colton model 216, Cherry-Burrell Corp., Park Ridge, IL 60068.
[2] CEA-06-125WT-350, Micro-Measurement, Romulus, MI 48174.
[3] Cable 8434-100, Belden Corp., Chicago, IL 60644.
[4] Model 13-4312-00, Gould Inc., Cleveland, OH 44117.
[5] EA-06-031De-120, Micro-Measurement, Romulus, MI 48174.
[6] Type NS-112, Dale Electronics, Norfolk, NE 68701.
[7] Model 5103N, Tektronix, Beaverton, OR 97077.
[8] ID data tablet/digitizer, Summagraphics Corp., Fairfield, CT 06430.
[9] C5A Camera/Land Pack Back, Tektronix, Beaverton, OR 97077.

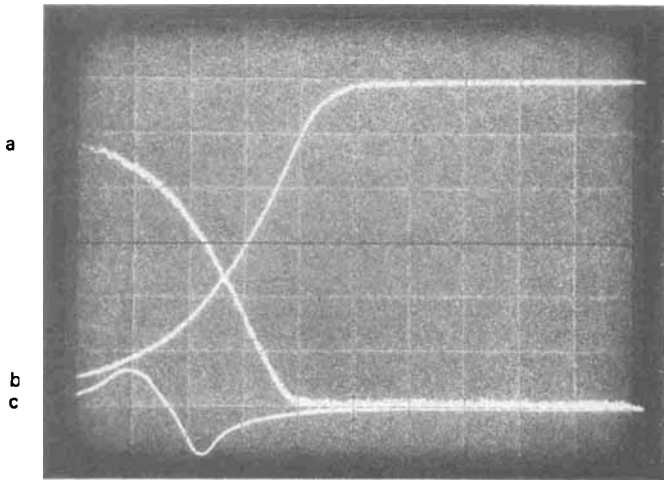

Figure 4—*Oscilloscope tracing of decompression and postcompression phases of sulfacetamide compression at a maximum pressure of 333 MPa at a sweep rate of 10 msec/division. Vertical deflections (division per volt) differ for the three traces: a, axial stress; b, radial stress; and c, turret rotation marker.*

example of these traces is shown in Fig. 4. When postcompression stress measurements were made over several minutes, the amplifier output signal was passed through a low-pass filter to reduce noise and to improve resolution.

Calibration—The instrumented die was calibrated under static conditions. A closely fitting rubber plug was placed in the die cavity, and known pressure was applied by loading weights onto a substitute upper punch in the form of a platform pedestal. A linear response was obtained, $r^2 = 0.989$, over the full range of 333 MPa.

Punch stress, as indicated by strain at the lower compression roller support rod, was calibrated against die wall stress under both static and dynamic conditions. In the latter case, the press was run at normal speed with a rubber plug in the die cavity. Oscilloscope traces of the simultaneously generated die wall and punch stresses were compared. Results obtained in this manner were indistinguishable from those observed when the turret was turned slowly by hand. Plots of die wall *versus* punch stress were linear with $r^2 \geq 0.999$.

Punch Displacement—It was not feasible to measure punch movement using a displacement transducer due to difficulty in mounting such a device. Instead, punch position, as a function of time, was calculated from tablet machine dimensions, turret velocity, and punch position relative to the compression rollers. The latter two quantities were computed from signals generated by a frame-mounted magnetic pickup in response to the passage of three turret-mounted permanent magnets. These were arranged so that one pulse was produced immediately prior to the compression event and two pulses after. Simultaneous punch and die stress curves for the compression of a rubber plug were symmetrical and exhibited maxima at the same time. Therefore, the punches were assumed to be centered between the compression rollers at the time corresponding to the common axis of symmetry of the stress *versus* time curves. The magnetic pickup signals were used as references for punch location, measurement of turret velocity, and triggering the oscilloscope.

The vertical displacement of the upper punch, z, as it passes under the compression roller (Fig. 5) is:

$$z = [(r_1 + r_2)^2 - x^2]^{1/2} \qquad \text{(Eq. 25)}$$

where r_1 and r_2 are the radii of the compression roller and the vertical curvature of the punch head rim, respectively; and x and x_2 are the horizontal distances between the vertical center lines of the compression roller and upper punch, respectively, and the center of vertical curvature of the punch head rim. The horizontal angle, ϕ, measured from the punch axis to the vertical centerline of the roller (Fig. 6) is a function of the turret angular velocity, ω. Thus, from Eq. 25, upper punch displacement at the position of greatest penetration into the die is:

$$z = [(r_1 + r_2)^2 - (r_3 \sin \omega t - x_2)^2]^{1/2} \qquad \text{(Eq. 26)}$$

where r_3 is the radial distance between the turret and punch axes. Equation 26 applies when the head of the punch, except for the flat, is in contact with the compression roller. During the period when the punch

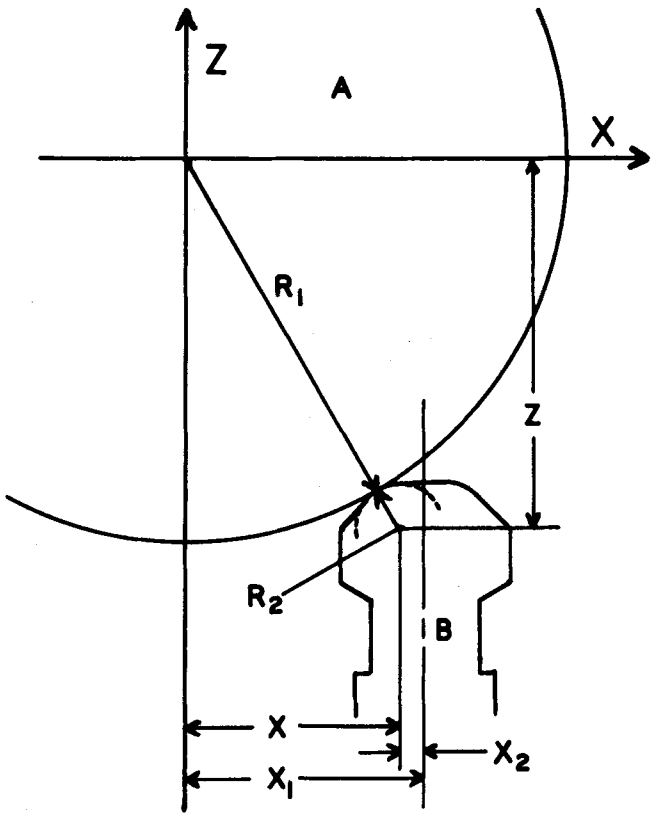

Figure 5—*Diagram of the geometric relationships between the compression roller (A) and punch (B) viewed from the side;* z, x, x_1, x_2, r_1, *and* r_2 *are as defined in Eqs. 25 and 26.*

head flat bears against the roller, the displacement equals r_1 plus r_2. This definition of displacement, z, is convenient for this study since it permits punch movements to be referred to the centers of the compression rollers.

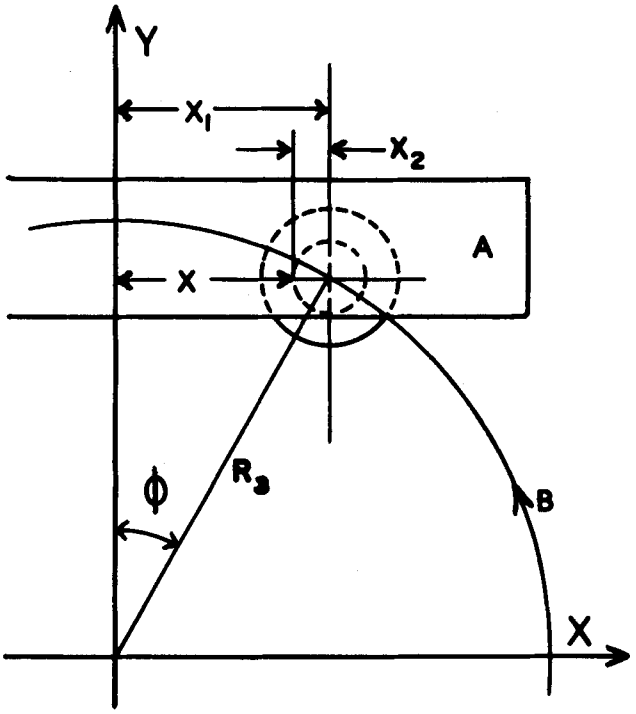

Figure 6—*Diagram of the geometric relationships between the compression roller (A) and the punch viewed from above. The vertical axis of the punch follows horizontal path B;* x, x_1, *and* x_2 *are as defined in Eq. 26.*

The punch displacement, z_0, at the instant the punches break contact with the tablet depends on the amount and the nature of the material in the die cavity. Taking into account the symmetry of compression by the upper and lower punches, the axial strain during the unloading phase is given by:

$$\epsilon_{zz} = \frac{2}{L}\{-[(r_1 + r_2)^2 - (r_3 \sin \omega t - x_2)^2]^{1/2} + |z_0|\} \quad \text{(Eq. 27)}$$

where L is the tablet thickness. When the flat region of the punch head is under the compression roller, axial strain is constant and equals:

$$\epsilon_{zz} = \frac{2}{L}[-(r_1 + r_2) + |z_0|] \quad \text{(Eq. 28)}$$

Stress Measurements—The die wall was lubricated prior to each compression by swabbing with a 10% slurry of magnesium stearate in ethanol. A precisely weighed amount of unlubricated powder was placed in the die cavity and leveled. The weight of the material was varied to achieve different compaction pressures. Each tablet was compressed in exactly the same location in the die, extending an equal distance above and below the radial stress-sensing element. The tablets were compacted at a turret velocity of 2.759 rad/sec and were allowed to remain in the die for several minutes until equilibrium radial stress was reached. Ejected tablets were ~5.5 mm in height, depending on fill weight and the material.

Stresses were recorded over the entire compaction cycle to obtain axial and radial pressure maxima. Separate recordings were made at faster scope sweep rates to provide better time resolution of the last 20–25 msec of the compaction cycle (the entire unloading period lasted ~30 msec) and the first 50–55 msec of the postcompaction period. Photographs of the scope tracings were digitized every 0.5 msec during unloading and every millisecond during postcompression. All experimentation was done in triplicate.

Materials—The materials to be compressed were dried in an oven at 145° for 2.5 hr and were stored over anhydrous calcium sulfate under vacuum until used. The compounds tested, microcrystalline cellulose[10], spray-processed lactose[11], and sulfacetamide[12], were otherwise used as received and were not mixed with a lubricant or other material prior to compression.

DATA ANALYSIS

Experimental data were analyzed using viscoelastic models which consisted of various combinations, in isostatic dilation and in distortion, of the basic models illustrated in Fig. 1. The simplest model yielding a good fit of the data was found to be elastic in dilation and Kelvin in distortion.

Unloading Phase—During the initial period of their withdrawal, the punches remain in contact with the tablet and, together with the die, prescribe its axial and radial strains, ϵ_{zz}, ϵ_{xx}, and ϵ_{yy}, respectively[13]. Superimposing the individual contributions of these strains to axial stress, using Eqs. 23 and 24, yields the expression:

$$(P'Q'' + 2P''Q')\epsilon_{zz} + 2(P'Q'' - P''Q')\epsilon_{xx} = 3P'P''\sigma_{zz} \quad \text{(Eq. 29)}$$

since, by symmetry, $\epsilon_{xx} = \epsilon_{yy}$. In the same manner, the equal radial stresses, σ_{xx} and σ_{yy}, can be obtained from Eqs. 23 and 24 in the form:

$$(P'Q'' - P''Q')\epsilon_{zz} + (2P'Q'' + P''Q')\epsilon_{xx} = 3P'P''\sigma_{xx} \quad \text{(Eq. 30)}$$

If it is assumed that the tablet is elastic in isostatic dilation and behaves as a Kelvin solid in distortion, $P'' = 1$ and $Q'' = q_0''$, while P' and Q' follow Eqs. 8 and 9. Substituting these expressions, together with Eq. 27, into Eqs. 29 and 30 provides equations for the axial and radial stresses during the experimentally imposed unloading conditions:

$$\sigma_{zz} = A_1 - A_2[(r_1 + r_2)^2 - (r_3 \sin \omega t - x_2)^2]^{1/2} + \frac{A_3 \omega r_3 \cos \omega t (r_3 \sin \omega t - x_2)}{[(r_1 + r_2)^2 - (r_3 \sin \omega t - x_2)^2]^{1/2}} \quad \text{(Eq. 31)}$$

where:

$$A_1 = (2/3)[(q_0'' - q_0')\epsilon_{xx} + (2q_0' + q_0'')|z_0|/L] \quad \text{(Eq. 32)}$$

$$A_2 = (2/3)(2q_0' + q_0'')/L \quad \text{(Eq. 33)}$$

$$A_3 = (4/3)q_1'/L \quad \text{(Eq. 34)}$$

and:

$$\sigma_{xx} = B_1 - B_2[(r_1 + r_2)^2 - (r_3 \sin \omega t - x_2)^2]^{1/2} - \frac{B_3 \omega r_3 \cos \omega t (r_3 \sin \omega t - x_2)}{[(r_1 + r_2)^2 - (r_3 \sin \omega t - x_2)^2]^{1/2}} \quad \text{(Eq. 35)}$$

where:

$$B_1 = (1/3)[(2q_0'' + q_0')\epsilon_{xx} + 2(q_0'' - q_0')|z_0|/L] \quad \text{(Eq. 36)}$$

$$B_2 = (2/3)(q_0'' - q_0')/L \quad \text{(Eq. 37)}$$

$$B_3 = (2/3)q_1'/L \quad \text{(Eq. 38)}$$

The macroconstants, A_i and B_i, of Eqs. 31 and 35 were determined from experimentally measured punch and die wall stresses by regression analysis (18). Equations 32, 33, 36, and 37 can be taken pairwise in any combination to calculate the microconstants, q_0' and q_0''. However, Eqs. 32 and 33 and Eqs. 36 and 37 are nearly parallel and were not paired for computation since the resulting calculated values of q_0' and q_0'' were sensitive to experimental error.

The vertical punch displacement at separation from the tablet, z_0, was determined from the time at which punch pressure fell to zero rather than from the macroconstants. Although z_0 values obtained by these two methods agreed within 0.05 mm, the latter method was less direct and was not used. For the same reason, ϵ_{xx} was calculated from measurements of ejected tablets rather than from Eqs. 32 and 36. Again, however, values obtained by the two methods agreed within ~0.05 mm.

Postcompression Phase—Radial stress and strain were the only variables measured directly during this period. Although a progressive change in the axial strain occurred, there was no means of reliably estimating it. Axial stress, however, can be estimated in various ways; because it is small in comparison with residual radial stress, effects of error are minor. Three hypotheses were tested in which axial stress was assumed to be either equal to zero, proportional to radial stress, or an exponentially decreasing function of time. Equations based on these assumptions were fitted to experimental data and showed the axial stress to be statistically indistinguishable from zero. From Eqs. 21 and 22, radial strain can be expressed as:

$$(2P''Q' + P'Q'')\sigma_{xx} + (P''Q' - P'Q'')\sigma_{zz} = 3Q'Q''\epsilon_{xx} \quad \text{(Eq. 39)}$$

If it is assumed that the tablet is elastic in dilation and Kelvin in distortion and if σ_{zz} is set equal to zero, Eq. 39 reduces to:

$$(q_0'' + 2q_0' + 2q_1' d/dt)\sigma_{xx} = 3q_0''(q_0' + q_1' d/dt)\epsilon_{xx} \quad \text{(Eq. 40)}$$

Integrating from time of punch separation, $t = 0$, to time t gives:

$$\sigma_{xx} = [\sigma_{xx}(0) - C_1]\exp(-C_2 t) + C_1 \quad \text{(Eq. 41)}$$

where:

$$C_1 = \frac{3q_0'q_0''\epsilon_{xx}(0)}{2q_0' + q_0''} \quad \text{(Eq. 42)}$$

$$C_2 = (2q_0' + q_0'')/2q_1' \quad \text{(Eq. 43)}$$

Equation 41 was fitted by nonlinear regression (19) to experimentally measured die wall stresses; C_1 is the equilibrium radial stress, and C_2 is the first-order rate constant for radial stress relaxation.

RESULTS AND DISCUSSION

The viscoelastic parameters of a tablet can be expected to depend heavily on the time course of compression and not solely on the chemical and physical nature of the powdered precursor. To investigate the effects of pressure, fill weights of the materials tested were adjusted to produce three pressure maxima: 125, 208, and 333 MPa. These pressures fall in the usual range for tablet compression. Test substances that differ in their compressibility were selected to provide for a sensitivity evaluation of the present method of data analysis to differences in material properties.

During the unloading period, the elastic behavior of the compacts predominated. This fact was evidenced by viscous contributions to the total distortion stress of ~1% only. Because the estimates of q_1'', calculated from A_3 and B_3, are of the same magnitude as the experimental error during this period, they are not reported. However, the relaxation pro-

[10] Avicel Ph 101, Food and Pharmaceutical Products Division, FMC Corp., Philadelphia, PA 19103.
[11] Fast-Flo Lactose, Foremost Dairies, Appleton, WI 54911.
[12] Ruger Chemical Co., New York, NY 07111.
[13] Subscripts refer to the reference axes of the compact, which are not necessarily labeled the same as in Eqs. 21–24.

Table I—Viscoelastic Constants [a] for Unloading and Postcompression Phases of Tablet Compression [b]

Viscoelastic Constant	Macroconstants [c]	Maximum Punch Pressure, MPa		
		125	208	333
		Microcrystalline Cellulose		
q_0'	A_1B_1	131 ± 6	169 ± 11	530 ± 20
q_0'	A_2B_2	132 ± 6	171 ± 11	529 ± 20
q_0''	A_1B_1	684 ± 32	1220 ± 82	2070 ± 78
q_0''	A_2B_2	687 ± 32	1220 ± 81	2050 ± 76
q_1'	$A_1B_1C_2$	0.844 ± 0.030	1.11 ± 0.05	3.83 ± 0.14
q_1'	$A_2B_2C_2$	0.858 ± 0.031	1.13 ± 0.05	3.79 ± 0.14
		Spray-Processed Lactose		
q_0'	A_1B_1	1180 ± 29	725 ± 13	1160 ± 15
q_0'	A_2B_2	1180 ± 29	727 ± 13	1160 ± 15
q_0''	A_1B_1	2120 ± 52	2400 ± 43	3000 ± 39
q_0''	A_2B_2	2120 ± 52	2410 ± 43	3010 ± 39
q_1'	$A_1B_1C_2$	3.79 ± 0.10	1.54 ± 0.06	2.10 ± 0.06
q_1'	$A_2B_2C_2$	3.80 ± 0.10	1.55 ± 0.06	2.11 ± 0.06
		Sulfacetamide		
q_0'	A_1B_1	25.7 ± 2.6	689 ± 21	28.2 ± 1.6
q_0'	A_2B_2	27.6 ± 2.6	691 ± 21	34.4 ± 2.0
q_0''	A_1B_1	986 ± 99	2050 ± 63	1730 ± 101
q_0''	A_2B_2	990 ± 95	2060 ± 63	1740 ± 100
q_1'	$A_1B_1C_2$	0.604 ± 0.035	9.19 ± 0.19	0.590 ± 0.022
q_1'	$A_2B_2C_2$	0.651 ± 0.036	9.24 ± 0.19	0.724 ± 0.027

[a] Calculated from mean macroconstants derived from triplicate compressions. [b] Units are MPa for q_0 and MPa sec for q_1. Standard errors are shown. [c] Macroconstants used in calculation of viscoelastic constants.

cesses that occur during the postcompression phase are kinetically dependent on viscous behavior and are largely controlled by it. The viscous microconstants, q_1', were calculated from C_2 and from the values of q_0' and q_0'' obtained during unloading (Table I).

Microcrystalline cellulose produced very strong tablets at all three pressures. These tablets exceeded the measurement range of the hardness tester[14]. All viscoelastic parameters increased with increased pressure. The elastic moduli were several times larger in dilation than in distortion, indicating that the material was more easily sheared than compressed. This latter behavior was observed for all three materials at all three pressures. In this regard, it is important to emphasize that a small elastic constant does not necessarily imply a small limiting stress at failure, and vice versa.

Tablets produced from spray-processed lactose also were very strong and exceeded the capacity of the hardness tester, except those produced at the lowest pressure. These latter tablets relaxed most slowly to their residual die wall pressures. This behavior was reflected by their relatively higher q_1' value shown in Table I.

The sulfas are noted for capping and splitting, which are often experienced in making tablets from them. With sulfacetamide, all three viscoelastic parameters passed through a maximum at intermediate pressures. Tablets produced at all three pressures were moderately strong and broke in the xz plane at about the same tensile stress of ~0.20–0.25 MPa. Tablets compressed at 208 MPa relaxed particularly slowly to equilibrium die wall stress. These tablets would be expected to be the most likely to cap had they been ejected at the normal time interval following compression.

The residual die wall stress at equilibrium, C_1, can be seen from Eq. 42 to be a function only of the elastic constants, q_0' and q_0'', and the radial strain, ϵ_{xx}. The rate constant, C_2, for the exponential decay of die wall stress is inversely proportional to q_1', as shown by Eq. 43. At the time of ejection from the die, the value of σ_{xx} is critical in determining if the tablet will fracture transversely (12) and exhibit capping or splitting.

Insight into tablet behavior during and after compression can be gained through viscoelastic parameters such as are examined in this study. However, the assumptions and approximations made in applying viscoelastic theory must be considered when interpreting the data. Although descriptive of fully dense materials, the theory also is able to accommodate porous materials. The mechanisms proposed for elastic yield or viscous flow in porous materials must be made in light of the influence of the voids. For example, in a porous solid, isostatic stress may cause fracture or plastic flow as the particles are forced into the pores. Under similar conditions and in the absence of fracture or flow, however, particles can elastically distort into voids. While shearing stresses can produce distortion solely through elastic deformations, they may also produce viscous flow. Distortion flow may be facilitated by voids and does not in itself reduce the void space available for the mass displacements that it produces.

This general behavior, elastic in dilation and Kelvin in distortion, was observed in the materials reported here. Although viscoelastic equations based on more complex models also correlated well with the stress/strain data, their use could not be justified because they did not significantly improve the fit between theory and experiment.

Further refinement of the theory to account for tablet anisotropy is possible but not currently feasible because of the limitations of present experimental methods. The number of viscoelastic parameters, arising from such anisotropic models, far exceeds the number of variables that can be measured simultaneously in the present apparatus. As a consequence, a set of indeterminate equations results. The models presented in this paper are being extended to a wider range of pharmaceutical solids and their mixtures.

[14] Pfizer, Pfizer Chemical Division, New York, NY 10017.

REFERENCES

(1) S. Shlanta and G. Milosovich, *J. Pharm. Sci.*, **53**, 562 (1964).

(2) E. N. Hiestand, J. E. Wells, C. B. Peot, and J. F. Ochs, *ibid.*, **66**, 510 (1977).

(3) S. Leigh, J. E. Carless, and B. W. Burt, *ibid.*, **56**, 888 (1967).

(4) J. E. Carless and S. Leigh, *J. Pharm. Pharmacol.*, **26**, 289 (1974).

(5) M. P. Summers, R. P. Enever, and J. E. Carless, *ibid.*, **28**, 89 (1976).

(6) E. Shotton, J. J. Deer, and D. Ganderton, *ibid.*, **15**, 106 (1963).

(7) E. L. Knoechel, C. C. Sperry, H. E. Ross, and C. J. Lintner, *J. Pharm. Sci.*, **56**, 106 (1967).

(8) K. Ridgway and P. H. Rosser, *J. Pharm. Pharmacol.*, **23**, 202S (1971).

(9) S. T. David and L. L. Augsburger, *J. Pharm. Sci.*, **66**, 155 (1977).

(10) T. Higuchi, T. Shimamoto, S. P. Eriksen, and T. Yashiki, *ibid.*, **54**, 111 (1965).

(11) J. E. Rees and P. J. Rue, *J. Pharm. Pharmacol.*, **30**, 601 (1978).

(12) W. M. Long, *Powder Metall.*, **6**, 73 (1960).

(13) J. S. Hardman and B. A. Lilley, *Nature*, **228**, 353 (1970).

(14) N. P. Suh, *Int. J. Powder Metall.*, **5**, 69 (1969).

(15) D. Train, *J. Pharm. Pharmacol.*, **8**, 745 (1956).

(16) D. R. Bland, "The Theory of Linear Viscoelasticity," Pergamon, New York, N.Y., 1960, pp. 1–17.

(17) W. Flugge, "Viscoelasticity," 2nd ed., Springer-Verlag, New York,

N.Y., 1975.
(18) N. H. Nie, C. H. Hull, J. G. Jenkins, K. Steinbrenner, and D. H. Bent, "Statistical Package for the Social Sciences," 2nd ed., McGraw-Hill, St. Louis, Mo., 1975.
(19) "Statistical Package for the Social Sciences; NONLINEAR Regression Subprogram," Vogelback Computing Center, Northwestern University, Evanston, Ill., 1978.

ACKNOWLEDGMENTS

Presented in part at the Basic Pharmaceutics Section, APhA Academy of Pharmaceutical Sciences, Anaheim meeting, April 1979.

Abstracted in part from a dissertation submitted by D. W. Danielson to the University of Minnesota in partial fulfillment of the Doctor of Philosophy degree requirements.

TLC Identification and GLC Determination of Meperidine and Its Metabolites in Biological Fluids

S. Y. YEH ˣ and H. A. KREBS

Received July 6, 1978, from the *National Institute on Drug Abuse, Division of Research, Addiction Research Center, Lexington, KY 40583.* Accepted for publication October 15, 1980.

Abstract □ Procedures were developed for TLC identification and GLC determination of meperidine and its metabolites, *i.e.*, *p*-hydroxymeperidine, normeperidine, and meperidinic and normeperidinic acids. Meperidine, *p*-hydroxymeperidine, and normeperidine were extracted with ether from biological fluids at pH 10, whereas meperidinic and normeperidinic acids and conjugated metabolites remained in the aqueous phase. The residue, upon evaporation of the extract to dryness, was derivatized with trifluoroacetic anhydride and gas chromatographed. Total (free and conjugated) meperidinic and normeperidinic acids in the aqueous phase were converted and determined as meperidine and normeperidine, respectively. A preliminary result of urinary disposition of meperidine and its metabolites in the rat is presented. The identity of these metabolites was confirmed with GLC–mass spectrometry.

Keyphrases □ Meperidine—and metabolites, TLC identification and GLC determination in biological fluids, rat, dog, and human □ Metabolites—meperidine, TLC identification and GLC determination in biological fluids of rat, dog, and human □ TLC—identification of meperidine and metabolites in biological fluids of rat, dog, and human □ GLC–mass spectrometry—determination of meperidine and metabolites in biological fluids of rat, dog, and human

The known major metabolites of meperidine are normeperidine and meperidinic and normeperidinic acids (1–4); *p*-hydroxymeperidine (5), meperidine *N*-oxide (6), hydroxymethoxymeperidine (7), *N*-hydroxynormeperidine (7), and *p*-hydroxynormeperidine[1] are minor metabolites (Scheme I). The hydrophilic and hydroxylated metabolites are excreted mainly in conjugated forms (1–3, 5, 7).

In earlier studies, radioisotopic and methyl orange dye methods (1–3, 8) were used to estimate meperidine and normeperidine in biological fluids. In later studies, meperidine, normeperidine, and *p*-hydroxymeperidine were estimated by GLC or GLC–mass spectrometry (9–19). Total meperidinic and normeperidinic acid were estimated as meperidine and normeperidine by methyl orange, GLC, and GLC–mass spectrometric methods after esterification (1–4, 9–20). This paper presents a simpler and more sensitive method for the determination of meperidine and its metabolites in biological fluids, primarily using GLC.

EXPERIMENTAL

Drugs—Meperidine hydrochloride[2], [*N-methyl*-^{14}C]meperidine hydrochloride[3] (3.4 mCi/mmole), normeperidine hydrochloride[2], *p*-hydroxymeperidine[4], and lidocaine hydrochloride[5] were used. The purity of the radiolabeled meperidine, determined by TLC with three solvent systems, was at least 98%. [*N-methyl*-^{14}C]Meperidinic, meperidinic, and normeperidinic acids were obtained by alkaline hydrolysis of their respective esters, and their purity was found to be 98% by TLC and GLC–mass spectrometry.

Meperidine *N*-oxide was synthesized by oxidation of meperidine (100 mg) by adding 85% *m*-chloroperbenzoic acid[6] (150 mg) in dried ether (2 ml) dropwise over 5 min. After the addition was completed, the solution was left at room temperature for 2 hr. Upon removal of the solvent, the residue was suspended in 2 ml of 10% potassium carbonate solution and extracted with ethylene dichloride containing 30% isopropyl alcohol (3 × 10 ml). Crystals were obtained upon concentration of the extract to ~1 ml. After cooling, centrifugation, and aspiration of the final drops of extract, the crystals were washed with ether and dried under vacuum, yielding 99 mg.

N-Hydroxynormeperidine was synthesized by oxidation of normeperidine with *m*-chloroperbenzoic acid (7). The final product was contaminated with normeperidine and other by-products but was sufficient for TLC and GLC–mass spectrometric identification.

GLC—The chromatograph[7] was equipped with flame-ionization detectors and 182-cm × 2-mm glass columns packed with 3% Poly I-110 coated on 80–100-mesh Gas Chrom Q. The temperatures of the oven, injector, and detector were 205, 225, and 250°, respectively. The gas flow rates of nitrogen, hydrogen, and compressed dry air were 30, 30, and 400 ml/min, respectively.

GLC–Mass Spectrometry—Chemical-ionization mass spectral data were obtained on a gas chromatograph–mass spectrometer[8] equipped with an interactive data system[9] and a 182-cm × 2-mm glass column packed with 3% Poly I-110 coated on 80–100-mesh Gas Chrom Q. The temperatures of the injector, column, and ion source were 230, 210, and 100°, respectively. Other specifications of the mass spectrometer were described previously (21).

TLC—Standard TLC procedures were followed. Aliquots (50 μl) of methanolic solution containing 50 μg of meperidine or its metabolites were spotted on instant thin-layer silica gel sheets[10] and linear, precoated glass silica plates[11]. Chromatograms were developed with one of the following solvent systems: A, *n*-butanol–water–acetic acid (35:10:3); B, ethyl acetate–ammonium hydroxide (17:1); C, ethyl acetate–methanol–ammonium hydroxide (17:2:1); D, benzene–methanol–diethylamine (48:1:1); E, *n*-butanol–3% ammonium hydroxide in water (50:50) using the upper phase; and F, ethyl acetate–diethylamine (17:1).

The chromatogram of nonlabeled standards was sprayed with iodo-

[1] Unpublished observations.
[2] Sterling-Winthrop Pharmaceutical Co., Rensselaer, N.Y.
[3] Mallinckrodt Chemical Co., St. Louis, Mo.
[4] Professor C. Lindberg, Department of Organic Pharmaceutical Chemistry, University of Uppsala, Uppsala, Sweden.
[5] Astra Pharmaceutical Products, Worcester, Mass.
[6] Practical grade, Aldrich Chemical Co., Milwaukee, Wis.
[7] Model 2700, Varian Aerograph, Varian Associates, Palo Alto, Calif.
[8] Model 3300, Finnigan Corp., Sunnyvale, Calif.
[9] Model 6000, Finnigan Corp., Sunnyvale, Calif.
[10] Gelman Instrument Co., Ann Arbor, Mich.
[11] Quantum Industries, Fairfield, N.J.

0022-3549/81/0500-0482$01.00/0